Characterizing the Influence of Turbulence Intensity on Energy Production at the Vineyard Wind 1 Farm

by

Emily P. Condon

B.S. Civil and Environmental Engineering
Massachusetts Institute of Technology, 2021

Submitted to the Department of Civil and Environmental Engineering
in partial fulfillment of the requirements for the degree of

Master of Engineering in Civil and Environmental Engineering

at the

MASSACHUSETTS INSTITUTE OF TECHNOLOGY

May 2022

Author .....
Department of Civil and Environmental Engineering
May 6, 2022

Certified by .....
Michael F. Howland
Assistant Professor of Civil and Environmental Engineering
Thesis Supervisor

Accepted by .....
Colette L. Heald
Professor of Civil and Environmental Engineering
Chair, Graduate Program Committee

Characterizing the Influence of Turbulence Intensity on Energy Production at the Vineyard Wind 1 Farm

by

Emily P. Condon

Submitted to the Department of Civil and Environmental Engineering
on May 6, 2022, in partial fulfillment of the
requirements for the degree of
Master of Engineering in Civil and Environmental Engineering

Abstract

Turbulence in the atmospheric boundary layer mitigates wake losses between turbines and is critical to power generation by wind farms. As offshore wind energy development increases in the United States, it is necessary to understand the impact turbulence intensity uncertainty has on predicting the annual energy production (AEP) of a wind farm. In numerical models used to calculate farm power, turbulence intensity is treated as a constant input, though it has variability in the physical atmosphere. Wind conditions, such as turbulence intensity, can be modeled with numerical weather prediction (NWP), or measured with *in situ* instruments that may not be available offshore in the exact location of interest. For the Vineyard Wind 1 offshore farm off the coast of Massachusetts, this uncertainty between data sources led to an overprediction of 4.4% by the NWP data compared to that of the *in situ* data. We found that assuming a median turbulence intensity, instead of the full turbulence intensity distribution, resulted in an AEP prediction difference of less than a third of a percent. While the quantitative results presented in this thesis are site-specific to the Vineyard Wind 1 farm, the results suggest that wind condition uncertainty has a significant impact on AEP uncertainty. The results motivate further *in situ* measurement campaigns to assess the wind conditions that offshore wind farms will encounter.

Thesis Supervisor: Michael F. Howland
Title: Assistant Professor of Civil and Environmental Engineering

Acknowledgments

In my efforts to earn a second degree from MIT, there is an institute full of people I must thank. To name a few:

Thank you to Professor Mike Howland for the opportunity to continue my education within this department, and for introducing me to the wonderful world of wind energy.

Thank you to my mentors and instructors within CEE, including Jesse Kroll and Heidi Nepf, who taught and supported me through my undergraduate education and beyond.

Thank you to my friends, co-counselors, teammates, and coaches who showed me how to make time for fun, even when the firehose was relentless.

Thank you to my parents, brothers, and family for their unconditional love and for letting me move to the other side of the country for five years.

Contents

List of Figures

List of Tables

Chapter 1

Background

1.1 Introduction to Offshore Wind

There is high potential to capture wind energy in offshore environments [1]. Recent infrastructure and energy diversification plans [2] have increased the desire to understand the wind energy resources on outer continental shelves (OCS) of the United States. The United States aim to deploy an offshore wind capacity of 30 gigawatts (GW) by the year 2030 and a capacity of 110 GW by 2050 [2]. In particular, the eastern coast has many lease areas already marked for offshore wind development, a proposed 16 wind farms with a total capacity of 26 GW [3]. Chosen for their high wind speeds, these regions have the potential to account for a significant percentage of energy supply in the adjacent communities and total energy production in each coastal state [3].

Compared to onshore environments, the offshore atmospheric boundary layer (ABL) has more stable conditions (i.e., less diurnal variability) caused by the heat capacity of water [4]. Higher wind speeds occur offshore due to less surface roughness over the ocean [4]. These two traits of the offshore environment make it a valuable resource for energy harvesting. The equation for power from a turbine is most generally

$$P = \frac{1}{2}\rho A C_P u^3 \tag{1.1}$$

in which power (P) is the product of air density (ρ), the swept rotor area (A), the coefficient of power (C_P), and the cube of the incoming wind speed (u).

It is important to understand and model the wind conditions offshore to best understand the potential power generation of that area. Though computational fluid dynamics (CFD) simulations can more accurately model flow through a wind farm, it is too expensive to run for optimization-oriented design decisions [5]. A more computationally efficient means of understanding offshore wind power potential is to use numerical-based methods. However, these numerical models may overlook certain key wind conditions. Additionally, because measuring wind conditions in areas of interest for offshore wind development is expensive, modelling technologies an alternate source for wind data. One example is numerical weather prediction (NWP), which utilizes mathematical models to predict future weather patterns based on historical data and models to interpolate where data is not available.

1.2 Vineyard Wind 1 Offshore Wind Site

This thesis focuses on the in-development Vineyard Wind 1 (VW1) offshore wind farm, the first federal utility-scale offshore wind energy project in the United States [6]. This wind farm is being developed in the federal lease area OCS-A-0501 off the coast of Massachusetts, 15 miles south of Martha's Vineyard. The project plan includes 62 General Electric Haliade-X 13-megawatt (MW) turbines spaced one nautical mile apart on an east-west, north-south grid. The current Vineyard Wind 1 development plans detail a capacity of 800 MW, powering over 400,000 homes in Cape Cod and other Massachusetts communities via Eversource, the local utility [6].

1.3 How Wind Farm Design Impacts Annual Energy Production

The annual energy production (AEP) of a wind farm is the amount of electrical energy generated over the course of a year. AEP is not only influenced by freestream

wind conditions, but also by how turbines in an array interact and impact downstream wind. Turbine wakes, the areas of low velocity downstream of a turbine due to extracting energy from the flow, are a function of wind conditions, which directly impact the performance of a wind farm [7]. Wind farm sites are often chosen for their high wind speeds, but wind conditions such as wind direction and turbulence intensity (TI) also play important roles in energy production. Wake interactions between turbines become larger at certain wind directions. Wake recharge, replenishing velocity downstream of a turbine with the above freestream flow, between turbines is directly linked to wind speeds and turbulence (e.g. [8], [9], [10]). Figure 1-1 shows contours of wakes in a turbine array with turbulence intensity varying from 6% to 50%. Higher TI leads to more wake recharge and greater power generation.

More turbines in a farm will increase the amount of energy harvested from the wind, but at an economic cost. The levelized cost of energy (LCOE) ($/MWh), the total cost of a wind farm capital and operational expenditures over the net AEP, is a tool to measure the trade offs between farm design and energy production. The reduction in LCOE for wind farms in recent decades have spurred widespread development of wind farms globally [7]. However, the LCOE for an individual development, such as the VW1 farm, is impacted by design decisions. Wind farms are often composed of tens to hundreds of turbines. A farm is designed based on constraints of total area available (wind farm footprint), type(s) of turbines, number of turbines, arrangement of turbines, and spacing between turbines [11]. Turbines can have different specifications such as rotor diameter, which dictates the total swept area of the blades, and hub height, the distance from sea level to the the turbine rotor center. The spacing between turbines is a balance between packing turbines tightly to maximize use of the lease area and spacing turbines apart to minimize wake interactions that influence downstream velocity deficits, the decrease in momentum downstream of a turbine due to energy extraction from the wind [11]. The distance between turbines therefore relates to the number of turbines that can fit within a given wind farm lease area. Adding more turbines may decrease total farm efficiency due to increased wake interactions. However, it may also reduce the LCOE, since the benefit of adding AEP

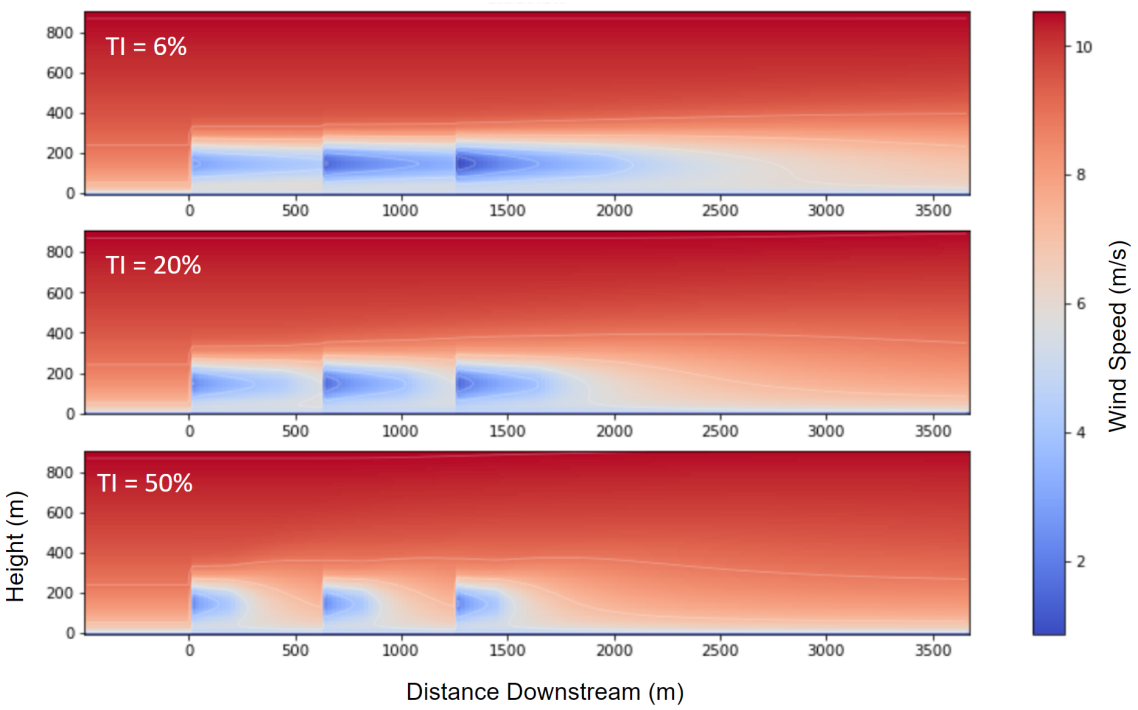

Figure 1-1: Sideview of a three-turbine wake interaction at constant wind speed and direction. As turbulence intensity (TI) increases, the velocities between turbines increases due to wake recharge induced by turbulent mixing. Note that 50% TI is not common.

outweighs the expense of each additional turbine.

In the atmospheric boundary layer, wind speeds typically increase with altitude, so wind farms developers often design farms with higher hub heights to capture those higher wind velocities. The wind speed relationship to altitude is often simplified with a power law

$$\frac{u}{u_r} = \left(\frac{z}{z_r}\right)^{\alpha} \tag{1.2}$$

in which u is the wind speed at height z, and u_r is the known reference velocity at height z_r. A high shear coefficient ($\alpha > 0.2$) is indicative of a stable atmosphere, while a low shear coefficient ($\alpha < 0.2$) characterizes an unstable atmosphere [4]. However, turbulence often decreases very rapidly with height, from a maximum value just above the land or ocean surface [4]. Due to this, it is important to investigate the relationships between wind speed, turbulence intensity, and AEP at the Vineyard Wind 1 site for different heights above sea level.

1.4 Low Turbulence Intensity

Turbulence, the irregular motion of a fluid, is important to large wind farms for recharging the velocity deficit, or wake, between adjacent turbines. Turbulence helps transport the kinetic energy from the freestream wind above the wind farm down to the rotor area where turbines can extract the energy, thus increasing power production [7]. Turbulent kinetic energy (TKE) is the root mean square of fluctuating wind velocity, for which σ_i^2 in Equation 1.3 represents the variance of the wind components.

$$\text{TKE} = \frac{1}{2}(\sigma_u^2 + \sigma_v^2 + \sigma_w^2) \tag{1.3}$$

Turbulence intensity (TI), or turbulence level, is the ratio of TKE to the mean wind speed ($\overline{u}$) [4]:

$$\text{TI} = \frac{\sqrt{\frac{2}{3}\text{TKE}}}{\overline{u}} \tag{1.4}$$

TI is a dimensionless parameter often expressed as a percent, with values below 5% considered relatively low and values above 10% considered relatively high [4]. TI affects wind farm performance by promoting wake deficit recharge downstream of turbines within a farm.

Though offshore sites typically have stronger and steadier wind speeds than onshore sites due to lower surface friction [12], the Vineyard Wind 1 site AEP may be significantly impacted by the low atmospheric turbulence observed in the region [12]. Bodini et al. (2019) analyzed lidar data from the Woods Hole Oceanographic Institute (WHOI) Air-Sea Interaction Tower (ASIT) and found "very low atmospheric turbulence" in this area.

1.5 Thesis Objective and Scope

The goals of this thesis are to explore the following questions:

Firstly, how does uncertainty in TI influence the farm's expected AEP? The uncertainty in TI comes from the availability of different data sources, in particular

the WHOI lidar data and the National Renewable Energy Laboratory (NREL) NWP data. The differences in TI data sources for the VW1 site may significantly increase the range of uncertainty for the farm's AEP. Additionally, how does AEP depend on using the median TI of a dataset versus the full probability distribution of TI?

Finally, what is the impact on AEP as TI is expected to decrease with height? Though wind speed increases with elevation, turbulence intensity decreases with height (something not often considered in wind farm modelling), which may impact the effectiveness of increased hub height on AEP.

Chapter 2

Methodology

2.1 Numerical Analysis in FLORIS

The FLOw Redirection and Induction in Steady State (FLORIS) [13], developed by NREL in collaboration with the Delft University of Technology, is a Python-based wind farm modelling software using steady-state wake models. During the course of this study, FLORIS version 3, a successor to FLORIS version 2.4, was released and all following numerical experimentation were done with the 3.0.1 update. FLORIS has previously been used in other offshore studies [14] and tested for sensitivity and uncertainty [15].

In this study, we used a numerical-based approach to model the VW1 wind farm. Because turbine power is a function of the area-averaged inflow velocity, it is necessary to understand the impact of turbulence intensity on turbine wakes, which is the velocity deficit downstream of turbines. We used a Gaussian wake model developed for FLORIS that is an integration of models from different papers, including Bastankhah and Porté-Agel (2014); Abkar and Porté-Agel (2015); Niayifar and Porté-Agel (2015); Bastankhah and Porté-Agel (2016); Dilip and Porté-Agel (2017). It is composed of a self-similar velocity deficit model [16] and elements of atmospheric stability. In their paper on analyzing heterogeneous wake using FLORIS, Farrell et al. (2021) translated the FLORIS methodology well from its Python environment [17].

The velocity deficit $u(x, y, z)$ is calculated with

$$\frac{u(x,y,z)}{U_\infty} = 1 - C\left[\exp\left(\frac{-(y-\delta)^2}{2\sigma_y^2}\right)\exp\left(\frac{-(z-z_h)^2}{2\sigma_z^2}\right)\right] \tag{2.1}$$

in which U_∞ is the incoming velocity; x, y, and z represent the spatial coordinates in the streamwise, spanwise, and vertical directions, respectively; δ is the wake deflection [18]; and z_h is the turbine hub height. C is the velocity deficit at the wake center:

$$C = 1 - \sqrt{1 - \frac{(\sigma_{y0}\sigma_{z0})C_0(2-C_0)}{\sigma_y\sigma_z}}, \text{ where } C_0 = 1 - \sqrt{1-C_T} \tag{2.2}$$

in which C_T is the thrust coefficient and σ is the wake width in the vertical (z) and lateral (y) directions. The wake widths are further dependent on the wake expansion rate, which is parameterized by k_y and k_z:

$$\frac{\sigma_z}{D} = k_z\frac{(x-x_0)}{D} + \frac{\sigma_{z0}}{D}, \text{ where } \frac{\sigma_{z0}}{D} = \frac{1}{2}\sqrt{\frac{u_R}{U_\infty + u_0}} \tag{2.3}$$

$$\frac{\sigma_y}{D} = k_y\frac{(x-x_0)}{D} + \frac{\sigma_{y0}}{D}, \text{ where } \frac{\sigma_{y0}}{D} = \frac{\sigma_{z0}}{D}\cosh\gamma \tag{2.4}$$

in which D is the rotor diameter, u_R is the velocity at the rotor, γ is the turbine yaw (in this study $\gamma = 0°$), and u_0 is the maximum velocity deficit in the wake. From Niayifar and Porté-Agel (2015), parameters k_y and k_z were estimated to be dependent on ambient incident turbulence intensity I_0, where $k_a = 0.38371$ and $k_b = 0.003678$ based on tuning using large eddy simulations of the neutral atmospheric boundary layer. The wake spreading rate can also be estimated based on power measurements [10]. Though k_y and k_z can potentially grow at different rates, they are set equal for model simplicity such that

$$k_y = k_z = k_a I + k_b. \tag{2.5}$$

The local turbulence intensity, I, is a combination of the ambient turbulence intensity with the wake-added turbulence, I_+ generated from the turbine operation.

FLORIS uses the following superposition methodology to calculate the total I:

$$I = \sqrt{\sum_{j=0}^{N} (I_{+j})^2 + I_0^2} \tag{2.6}$$

in which N is the number of turbines upstream that generate added turbulence intensity. The Crespo-Hernandez wake turbulence model [19] was used to calculated added turbulence intensity:

$$I_+ = 0.73 a^{0.8325} I_0^{0.0325} (x/d)^{-0.32} \tag{2.7}$$

in which a is the axial induction factor and x is the distance downstream..

2.2 FLORIS Validation

Using data and methods from existing literature, we validated FLORIS methodology by comparing our power outputs to those from a well-studied wind farm. Niayifar and Porté-Agel [9] compared their new power model against large eddy simulation (LES) data for the Horns Rev wind farm off the coast of Denmark. Using the study's input parameters (i.e., farm layout, turbine specifications, wake model parameters), we compared the FLORIS power output against that of the Horns Rev numerical analysis. The Gaussian wake velocity model detailed in section 2.1 was used. Two numerical experiments were performed to compare the Niayfar Horns Rev power data to the FLORIS power outputs. The first was comparing normalized power per row at a constant wind speed, direction, and TI (Figure B-1). The second compared normalized power at a constant wind speed and TI at wind directions sweeping 173° to 353° (Figure B-2). The results showed that FLORIS slightly underpredicts power output per row but maintained the shape of the original Horns Rev plots. Because the goals of this thesis are to compare AEP of different datasets, we hypothesize that a consistent underprediction is therefore not expected to significantly impact relative comparisons.

2.3 Wind Farm Specifications

The Vineyard Wind 1 analysis was performed using an array of turbines spaced one nautical mile, or 8.5 rotor diameters, apart as shown in Figure 2-1. The plans for the Vineyard Wind 1 farm include 62 General Electric Haliade-X 13MW turbines, which have a hub height of 135m and a 218m rotor diameter. However, the power and thrust data for these turbines are not publically available. Therefore, this study uses International Energy Agency (IEA) 15MW reference turbines, commonly used in studies done by NREL [20]. The IEA 15MW turbine has similar rotor diameter (240m) and standard hub height (150m) as the Haliade-X 13MW turbine.

The IEA 15MW turbine thrust and power curves are shown in Figure 2-2. The power curve predicts the turbine's power at each wind speed. These curves are divided into three regions. Region 1 is from wind speeds of 0 m/s to the cut-in speed (3 m/s for the IEA 15MW turbine), the speed at which the turbine starts generating power. Region 2 is from the cut-in speed to the rated wind speed (10.6 m/s for the IEA 15MW turbine), the speed at which the rated (maximum) power is reached. Past the rated wind speed is Region 3, throughout which the turbine actively slows itself down to limit fatigue.

2.4 Wind Condition Data Sources

For this study, two data sources were compared: *in situ* lidar measurements and modelled weather prediction data.

2.4.1 WHOI ASIT Lidar Data

The Woods Hole Oceanographic Institution's (WHOI) Air-Sea Interaction Tower (ASIT), located at 41°19.501'N, 70°34.000'W, is a cabled, fixed platform located approximately 3 km south of Martha's Vineyard that has been collecting continuous observations of the atmospheric boundary layer since 2016. Bodini et al. [12] used data from October 2016 to October 2017 to analyze the turbulence intensity offshore

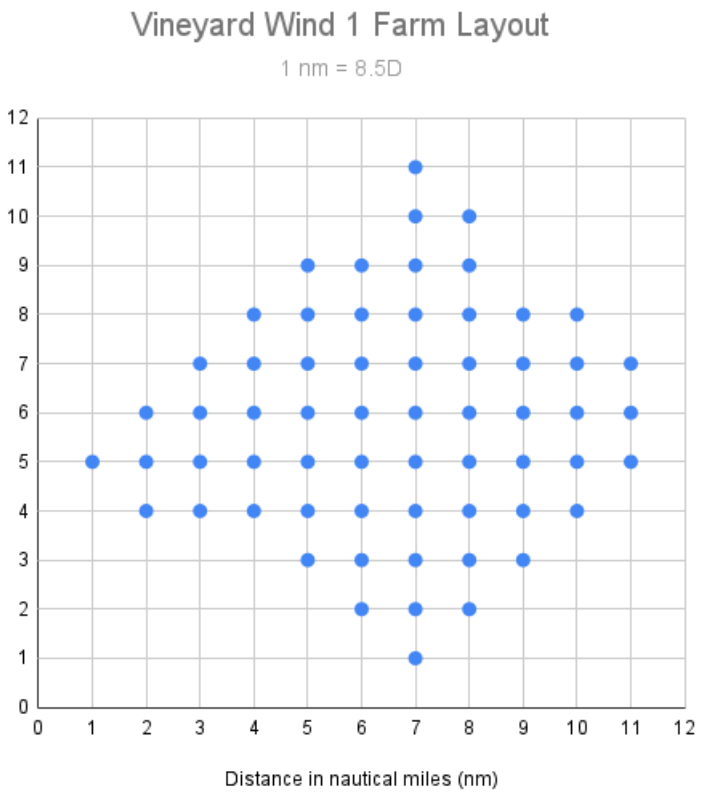

Figure 2-1: Vineyard Wind 1 Farm Layout – an array of 62 turbines spaced 1 nautical mile apart.

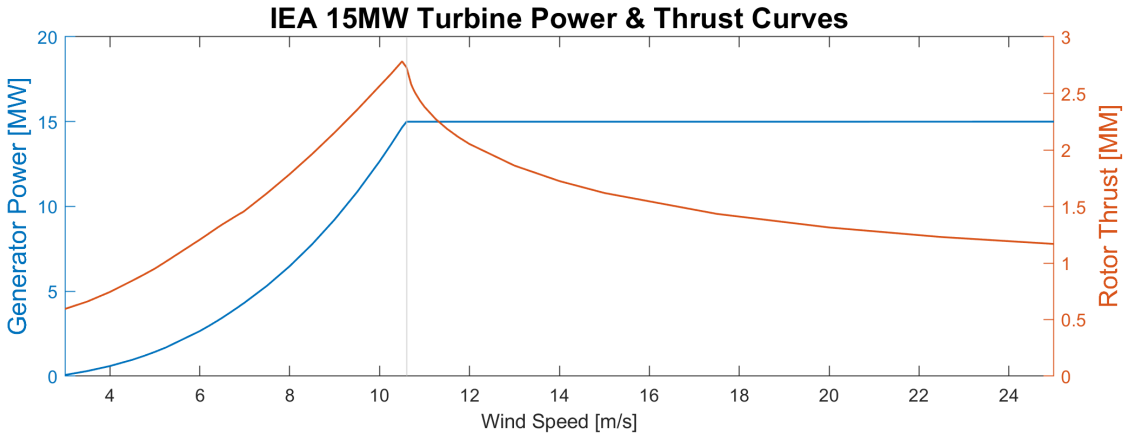

Figure 2-2: IEA 15MW turbine power and thrust curves, data from NREL [20]. The grey vertical line indicates the rated power speed 10.6 m/s. Region 2 (left of the vertical line) is from cut-in speed (3 m/s) to rated speed; power is zero at speeds less than cut-in. Region 3 (right of the vertical line) shows the range of wind speeds for rated power.

of the East Coast of the United States. Periods during which rain was observed have been excluded from Bodini's dataset. Because of its proximity to land at its north, the ASIT wind speed and turbulence kinetic energy (TKE) measurements may not be appropriate for understanding northerly wind over the open ocean [12]. However, this thesis is concerned with understanding how the currently available measurement data may be used to predict wind farm annual energy production and influence wind farm siting and design.

The data used in this analysis are from Bodini's processed data [21] from the "MetOcean Initiative" funded by the Massachusetts Clean Energy Center [22]. The data, collected with lidar, contain wind direction, wind speed (m/s), and turbulence kinetic energy (m^2/s^2). The lidar took measurements at the following elevations above sea level in meters: 53, 60, 80, 90, 100, 120, 140, 160, 180, and 200.

2.4.2 NREL Wind Prospector Data

Being able to quantify this energy potential without relying on *in situ* measurements has led to the development of methodologies and public datasets, such as those provided by NREL. In 2013, NREL began developing the Wind Integration National Dataset (WIND) Toolkit [23], the largest publicly available grid integration wind dataset, with seven years of data at 5-minute and 2 km x 2 km resolution over 126,000 sites. In 2020, NREL released the Offshore Mid Atlantic Dataset, an updated 21-year (2000-2020) wind resource set that replaced the WIND Toolkit for the offshore Atlantic region [23]. This new dataset used a more recent version of Weather Research and Forecasting (WRF) NWP, version 4.1.2.

For this study, the data was taken from coordinates within the VW1 lease area, 40°55.571'N, -70°42.134'W. The relevant attributes from the Wind Prospector (WP) Offshore Mid Atlantic dataset included wind direction (degrees), wind speed (m/s), and turbulence kinetic energy (m^2/s^2), each collected at 5-minute intervals. Each wind condition is available for the following elevations above sea level in meters: 10, 20, 40, 60, 80, 100, 120, 140, 160, 180, 200, 220, 240, 260, 280, 300, 400, and 500.

2.4.3 Data Processing

For the current study, a year's worth of data from October 2016 to September 2017 was collected and sorted such that the WHOI lidar data and Wind Prospector NWP data had measurements at the same 10-minute time steps. The WP data, taken at 5-minute intervals, were averaged to obtain the 10-minute resolution. Because the WHOI data was processed by Bodini et al. (2019), the times when precipitation occurred were omitted. These times and any other gaps in WHOI data were similarly omitted from the WP data.

For each dataset, turbulence intensity, the relative fluctuation of wind velocity versus the mean wind speed, was calculated. Turbulence intensity (TI) can be derived from TKE via Equation 1.4 with 10-minute wind speed averages.

2.5 Numerical Experiments

To investigate the uncertainties in wind condition data sources, we ran controlled numerical experiments using the FLORIS software. The Vineyard Wind 1 farm orientation with 62 IEA 15MW turbines was initialized. The turbines are fully yaw aligned, such that the rotors are fully facing the incoming wind regardless of wind direction. In the physical ABL, the presence of the ground (or ocean surface) creates friction that forces a velocity profile that is zero at the lower boundary layer and increases with height [4]. However, for these analyses, wind shear was omitted, meaning that the incoming velocity does not change with height in this model. Because of this, the "hub height" of the farm is set by the elevation of the wind condition measurements (e.g., lidar data recorded at 140m will result in an AEP calculation of turbines with hub height 140m).

2.5.1 Additions to FLORIS Code

FLORIS uses wind speed and direction distributions in power calculations, but turbulence intensity distributions are not considered. Instead, TI is prescribed as a constant

value for all inflows. For this study, additions have been made to the existing FLORIS package to include TI probability distributions. For the typical FLORIS setup, wind conditions for the inflow are initialized; wind speed and direction inputs may be heterogeneous vectors, but TI can only be inputted as a singular value. FLORIS uses the Gaussian wake model detailed in Section 2.1 to calculate the incident wind speed felt by each turbine in the farm, and the individual turbine powers, measured in Watts, (Equation 1.1) are determined with the rotor area-averaged velocity. The total farm power is the sum of the individual turbine powers. AEP, often measured in gigawatt-hours (GWh), is then calculated using the mean farm power multiplied by 8760 hours (the number of hours in a year).

In order to fully capture the TI distributions from the wind condition datasets, we iterated the turbine power calculation over the entirety of the three-variable (wind speed, wind direction TI) inflow combinations. Unlike the default FLORIS methods, each farm power was calculated using a different inflow TI value. Similar to the above methods, AEP (called "full AEP" in the remainder of this study) was then calculated using the mean farm power.

2.5.2 Farm Efficiency Analyses

Farm efficiency is the ratio between the total farm power and the maximum potential farm power without wake losses. The farm efficiency was calculated using the total farm power over the power of the freestream operating turbine (the turbine at the beginning of the inflow) multiplied by the number of turbines in the farm. To understand the impact of using the full TI probability distribution versus the singular median TI value, we ran three different farm efficiency analyses. The first used only the median values for all three wind conditions: wind speed, wind direction, and TI. The second was based on the standard FLORIS methodology, using the median value for TI and the full wind speed and direction probability distributions. The final analysis was based on our additions to the FLORIS code, using the full probability distributions for each wind condition to find the "full" farm efficiency.

2.5.3 Monte Carlo Sampling for Probability

It is computationally expensive to run power calculations for each of the wind conditions, which can number to 52,560 for a year's worth of 10-minute samples. The machine used in this analysis had an Intel Core i7, 3.8 GHz processor and required approximately 12 hours per 30,000 wind condition iterations. To combat the dimensionality of the added TI variable and find the statistical significance of a more efficient method, Monte Carlo estimation was used. Monte Carlo uses random sampling to draw inferences about a population; as the sample size from a distribution grows, the average of the samples grow closer to the true mean of the population [24]. In our study, the number of samples was chosen, and that number of random indices from the wind condition data were used in the wake model. In practice, the goal was to determine the minimum number of wind condition samples required to get reasonably close to the full AEP.

Chapter 3

Results

3.1 Differences Between TI Datasets

Table 3.1 shows the farm efficiency of the Vineyard Wind 1 setup at different prescribed turbulence intensities at constant wind speed (8 m/s) and direction (270°). Farm efficiency increases non-linearly as turbulence intensity increases.

Turbulence Intensity	**Farm Efficiency**
0.02	60%
0.04	67%
0.06	71%
0.08	75%
0.1	78%
0.2	88%

Table 3.1: Farm efficiency at prescribed turbulence intensities for the Vineyard Wind 1 farm.

The processed and matched time-stamp wind speed and turbulence intensity data for the WP and WHOI datasets are shown in Figure 3-1. Visually comparing the wind directions, the WP wind roses (Figures 3-1a and 3-1b) show more westerly winds while the WHOI wind roses (Figures 3-1c and 3-1d) have predominately southwesterly winds. The WP has generally lower turbulence intensities than WHOI, though they both show the lowest turbulence intensities coming from the southwest.

Figure 3-2 shows contour maps of the relationships between each inflow wind

(a) WP Wind Speed

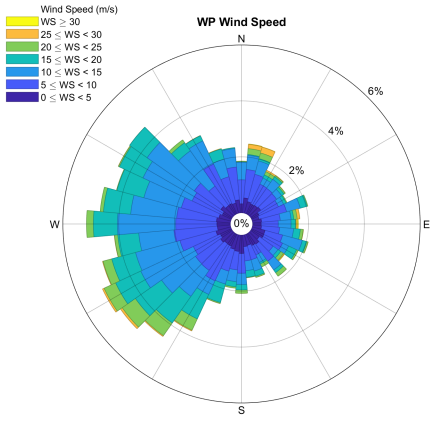

(b) WP Turbulence Intensity

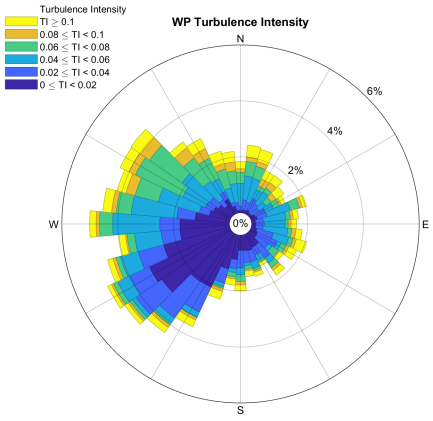

(c) WHOI Wind Speed

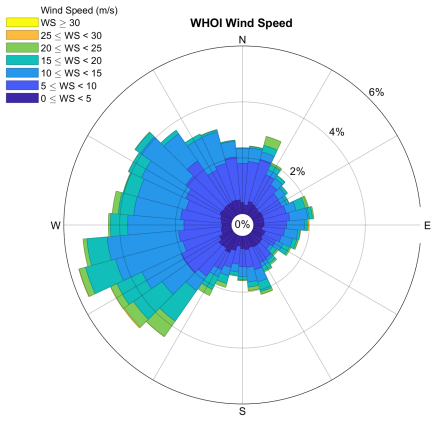

(d) WHOI Turbulence Intensity

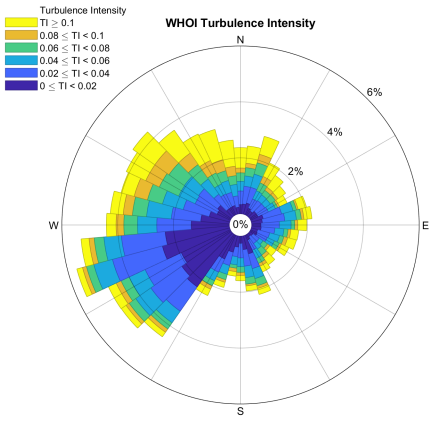

Figure 3-1: Wind roses for wind speed and turbulence intensity at 140m. Figures a) and b) are from the Wind Prospector dataset; c) and d) are measured by the WHOI ASIT lidar.

condition. The resolution of each wind condition is as follows: 1 m/s wind speed, 3° wind direction, 0.01 turbulence intensity. In Figure 3-2a, only the region two range of the turbine power curve (cut-in speed 3 m/s to rated-power speed 10.6 m/s) is shown, as farm efficiency tends towards 100% when the wind speed is above rated power speed. This is shown with wind speed on the vertical axis in Figure 3-2c. In Figures 3-2b and 3-2c, the farm efficiency is lowest when wind directions are aligned with rows or columns of the turbine array and turbine wakes are directly interacting and reducing wind speeds between turbines.

To better understand the differences in the wind condition distributions of each dataset, the histograms in Figure 3-3 show overlapping probability distributions. For all wind condition pairs, the two-sample Kolmogorov-Smirnov test null hypothesis stating that the data are from the same continuous distribution was rejected at the 5% confidence level. Therefore, the datasets are statistically different. The WP data show more instances of higher wind speeds than the WHOI data. Additionally, the WP turbulence intensities have two peaks at 0.02 and 0.05, while the WHOI TI peaks at 0.02 only. Table 3.2 shows the mean, median, and standard deviation (σ) for each dataset and wind condition. The medians for wind speed and wind direction are similar to each other, while the turbulence intensity medians are identical.

	Wind Direction			**Wind Speed (m/s)**			**TI**		
	mean	median	σ	mean	median	σ	mean	median	σ
WP	209.4°	233.0°	97.6°	10.6	10.0	5.4	0.05	0.04	0.09
WHOI	209.5°	236.9°	100.8°	10.0	9.4	4.9	0.06	0.04	0.07

Table 3.2: Statistics of the WP and WHOI wind condition data at 140m elevation. Number of data point timestamps = 32948.

(a) Turbulence Intensity vs Wind Speed

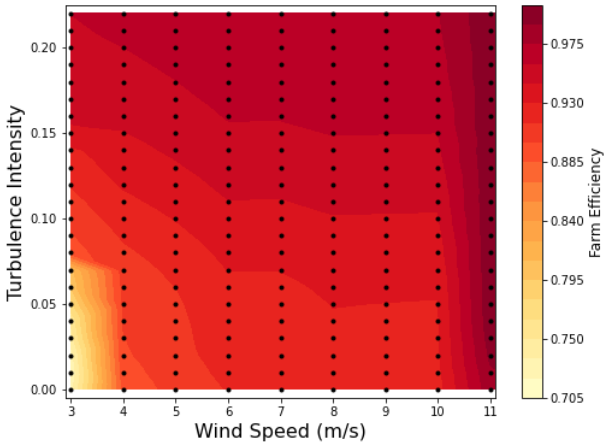

(b) Turbulence Intensity vs Wind Direction

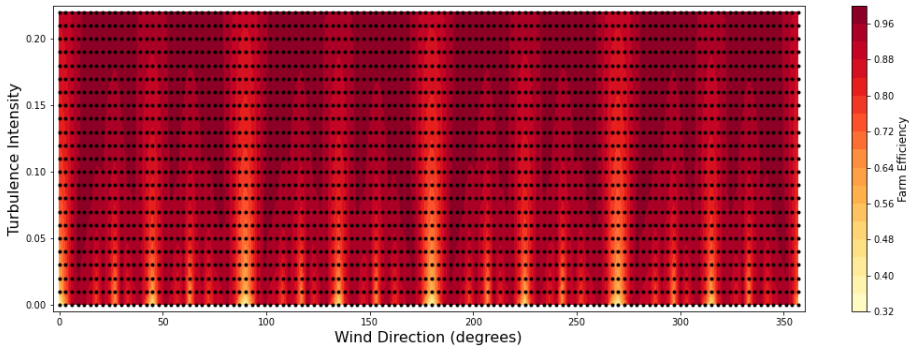

(c) Wind Speed vs Wind Direction

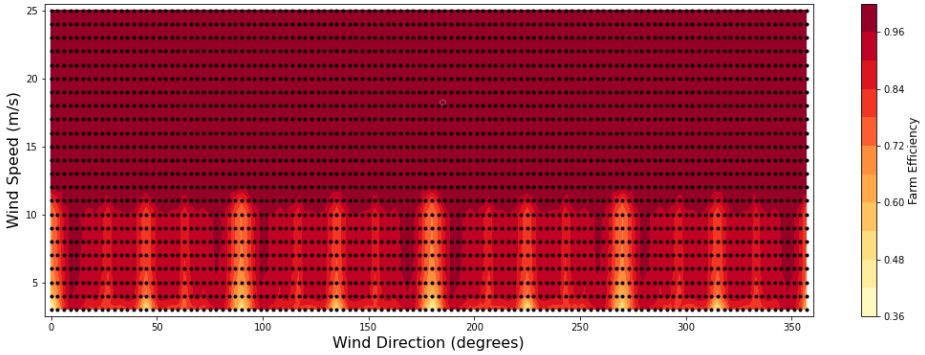

Figure 3-2: Contour plots comparing the farm efficiencies of each combination of wind conditions. Figure 3-2a focuses on the power curve region 2 range of wind speeds. When wind conditions are fixed: wind direction is 240°; wind speed is 8m/s; TI is 8%.

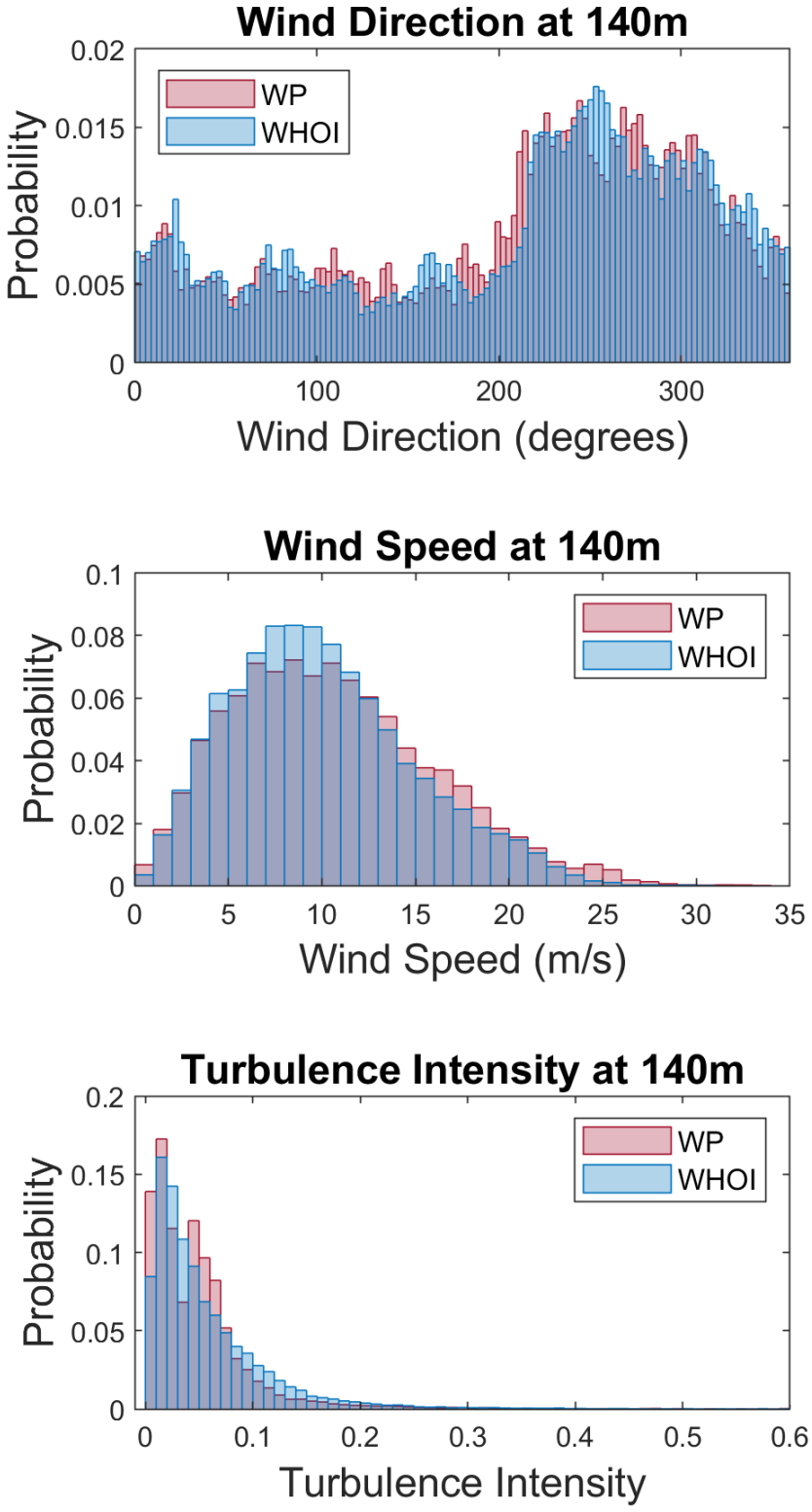

Figure 3-3: Overlapping histograms of WP and WHOI data at 140m for wind direction, wind speed, and TI.

The Monte Carlo random sampling scheme is shown in Figure 3-4 with the following sampling sizes: 100, 1000, 5000, 10000, 20000, 30000, 40000, 60000. Each sample size was iterated 10,000 times, and the mean and range of percent difference from the full calculated AEP is plotted. The full calculated AEP for the WP and WHOI data at 140m is 5355.21 GWh and 5129.68 GWh, respectively. Figure 3-5 shows the differences between the random sampling in the previous figure.

$$\% \text{ Difference} = \frac{|\text{WHOI} - \text{WP}|}{\text{WHOI}} \cdot 100 \tag{3.1}$$

The percent difference (Equation 3.1) between the AEP values for the WP and WHOI datasets is 4.40% in favor of the WP AEP, shown in Figure 3-5 as the red reference line.

(a) WP AEP Monte Carlo Integration (b) WHOI AEP Monte Carlo Integration

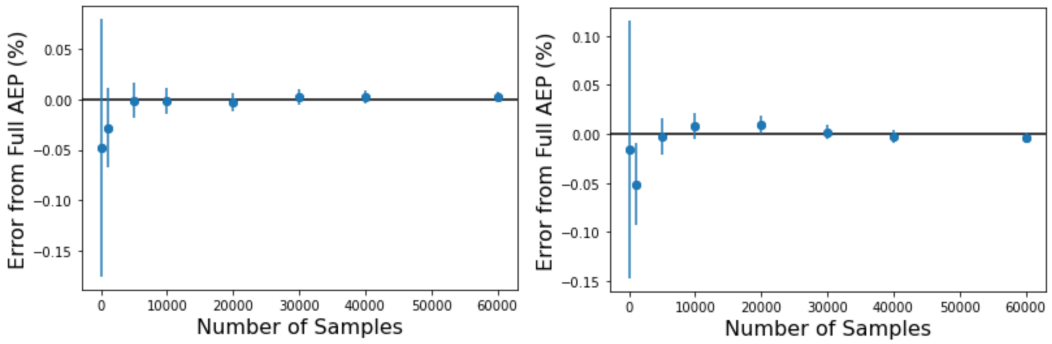

Figure 3-4: Random sampling mean percent difference from the full calculated AEP for each dataset. Bars indicate range of percent difference for 10,000 iterations of each sample amount.

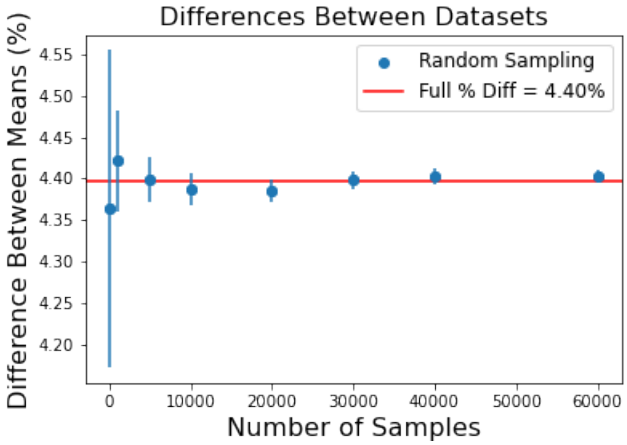

Figure 3-5: AEP differences between datasets. Red line indicates the percent difference (Equation 3.1) between the full calculated AEP.

3.2 Changes in Hub Height

Similar results were found with the datasets at increased hub heights of 160m, 180m, and 200m. The processed wind speed data for the WP and WHOI datasets are shown in Figure 3-6. For all wind conditions and hub heights, the WP and WHOI data were statistically different. Visually comparing the wind directions, the WP wind roses show consistent westerly winds with height while the WHOI wind roses have southwesterly winds that become more westerly with height. In Figure 3-7, the turbulence intensities qualitatively do not change with height for each dataset. For both datasets, the wind speed gradually increases as elevation increases (Appendix A), though the median turbulence intensities remain constant. The full histograms can be viewed in Appendex B.

The full AEP was calculated for the WP and WHOI datasets at each hub height and are shown in Figure 3-8. AEP increases with height for both, and the percent difference between the two shrink.

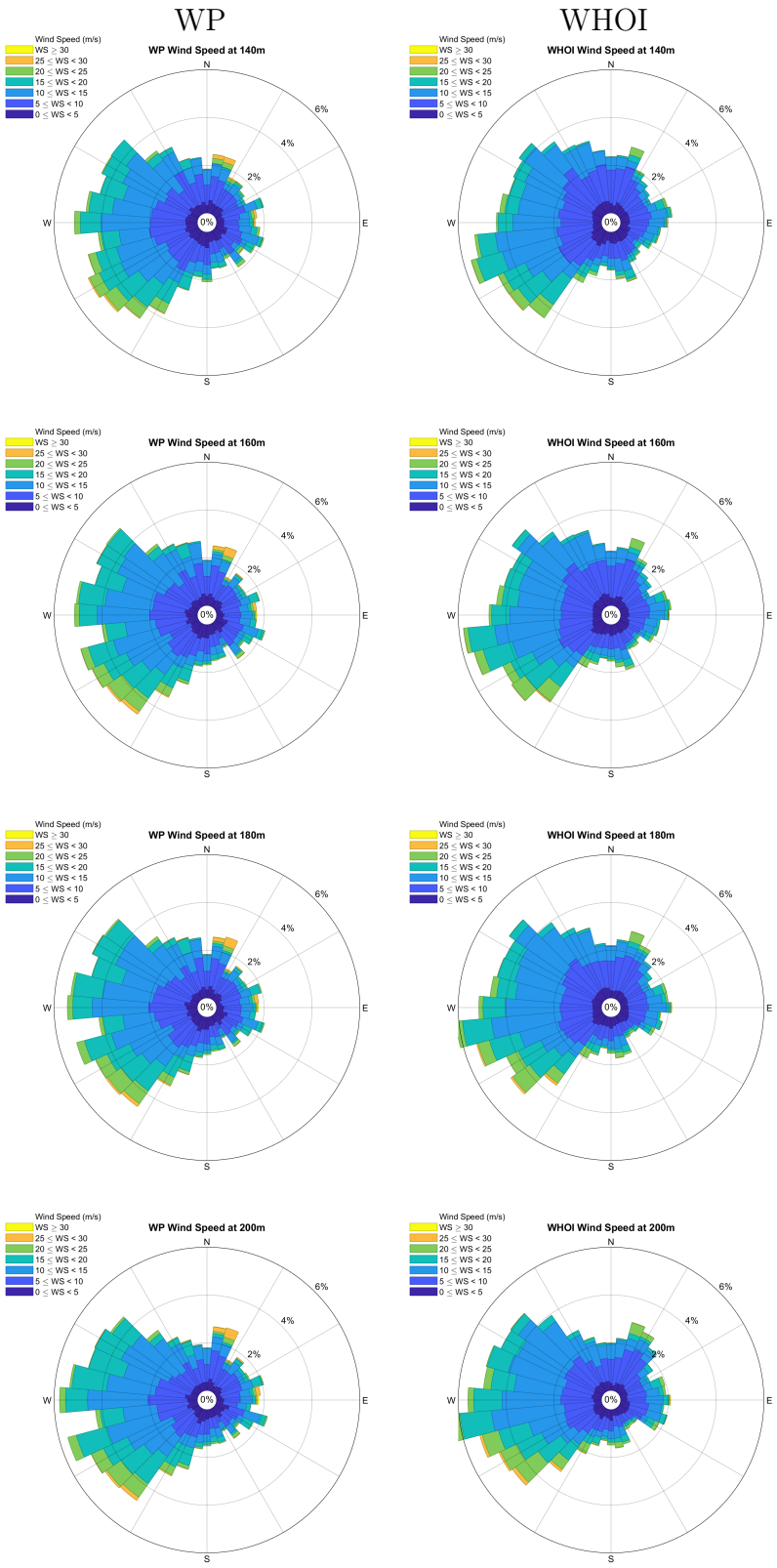

Figure 3-6: Wind roses for wind speed at the hub heights 140m, 160m, 180m, 200m for WP (left) and WHOI (right).

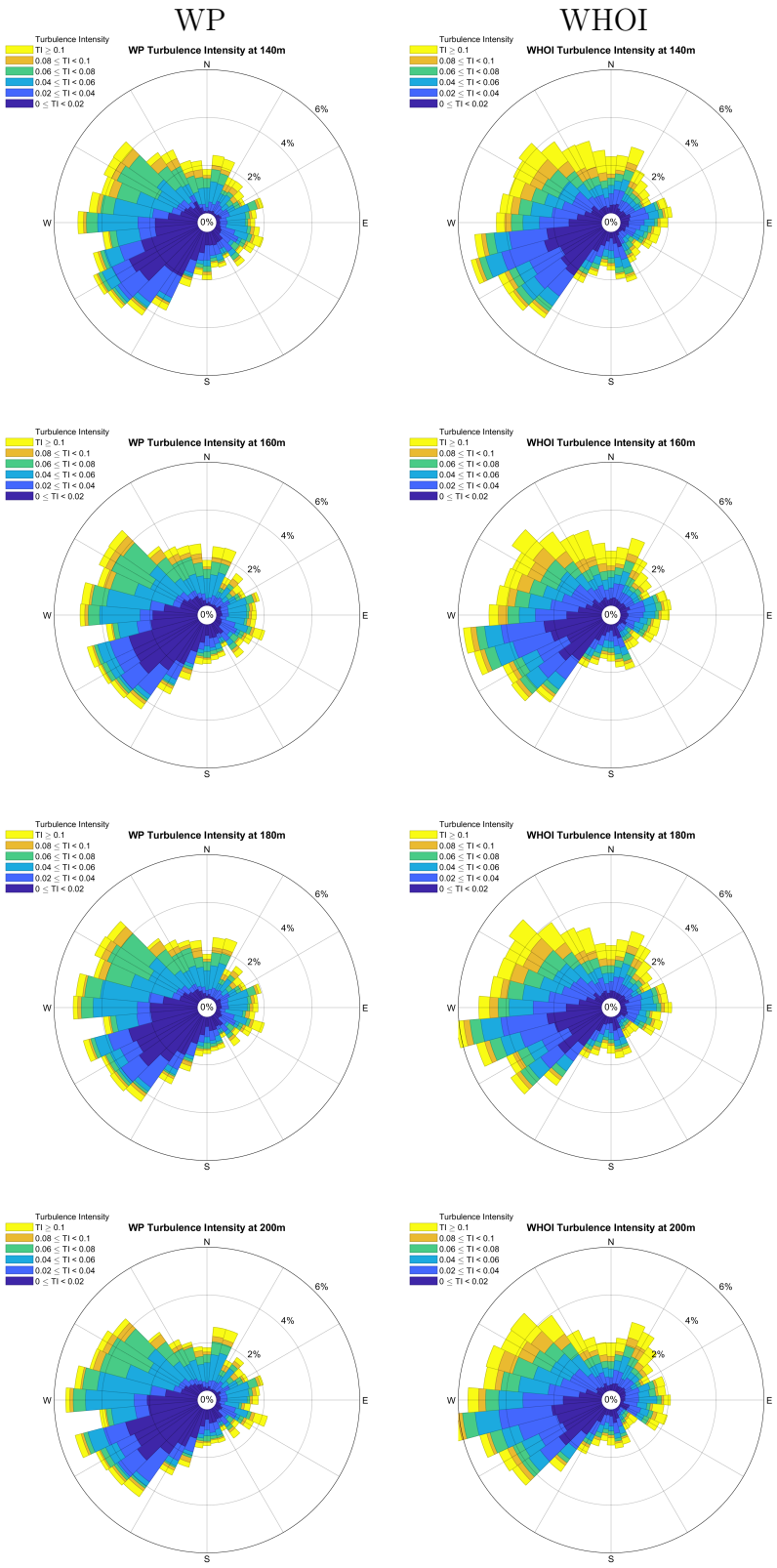

Figure 3-7: Wind roses for turbulence intensity at the hub heights 140m, 160m, 180m, 200m for WP (left) and WHOI (right).

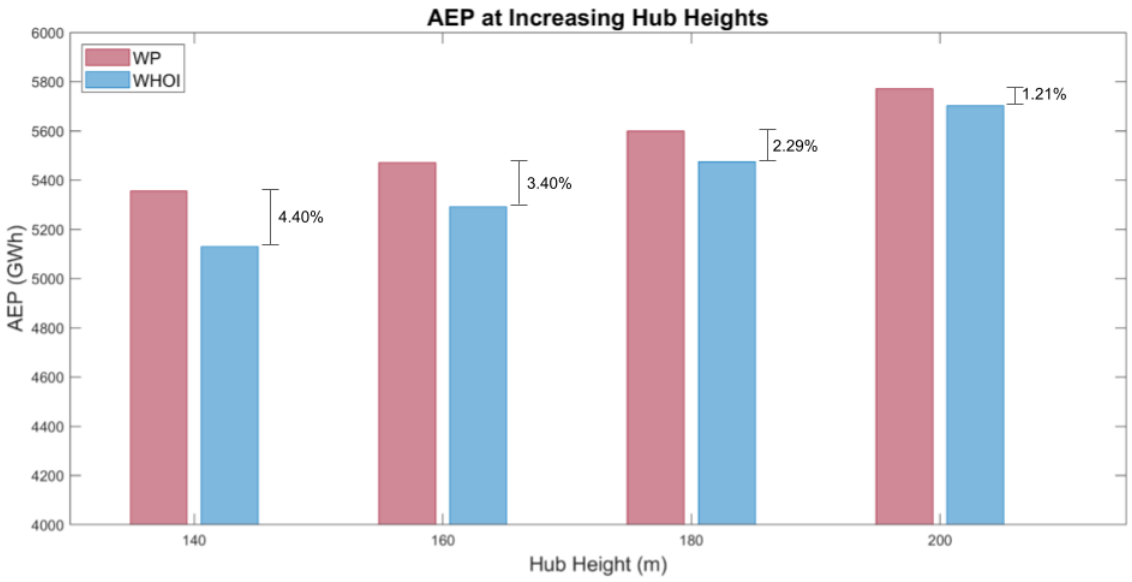

Figure 3-8: Calculated AEP at increasing hub height for each dataset. Percent differences (Equation 3.1) between datasets at each height is labeled.

3.2.1 Median TI vs Full TI Distribution

Tables 3.3 and 3.4, WP and WHOI, respectively, show the results of the farm efficiency experiments for different hub heights. The corresponding AEP values are located in the Appendix (Tables A.4 and A.5).

WP Farm Efficiency			
Hub Height	**1) Median TI, WS, WD**	**2) Median TI; Full WS & WD**	**3) Full TI, WS, WD**
140m	94.88%	88.29%	88.36%
160m	90.24%	88.88%	88.96%
180m	93.91%	89.31%	89.41%
200m	93.91%	89.85%	89.98%

Table 3.3: Farm efficiency of the VW1 farm using the WP data at different hub heights. Farm efficiency 1) uses the median values for TI, wind speed (WS), and wind direction (WD); 2) uses the median TI with the full probability distributions of WS and WD; 3) uses the full probability distributions for TI, WS, and WD.

WHOI Farm Efficiency			
Hub Height	**1) Median TI, WS, WD**	**2) Median TI; Full WS & WD**	**3) Full TI, WS, WD**
140m	90.76%	88.00%	88.82%
160m	92.36%	88.47%	89.44%
180m	79.15%	88.88%	89.96%
200m	79.60%	89.57%	90.68%

Table 3.4: Farm efficiency of the VW1 farm using the WHOI data at different hub heights. Farm efficiency 1) uses the median values for TI, wind speed (WS), and wind direction (WD); 2) uses the median TI with the full probability distributions of WS and WD; 3) uses the full probability distributions for TI, WS, and WD.

Chapter 4

Discussion

4.1 TI Data Source vs. AEP at 140m Hub Height

As seen in Table 3.1, turbulence intensity has a direct influence on wind farm power efficiency. Farm efficiency significantly increases as turbulence intensity increases at constant wind speed and direction, since turbulent mixing recharges the wake velocity deficit downstream of a turbine. It is therefore significant to include TI in energy modelling calculations.

The wind roses in Figure 3-1 show distinct differences in the magnitudes and directions of wind speeds and turbulence intensity between the two datasets. The WP wind roses (Figures 3-1a and 3-1b) show a spread of wind directions coming from the northwest, west, and southwest. The WP wind speeds more often reach velocities of 20 m/s and higher. Comparatively, the WHOI data (Figures 3-1c and 3-1d) has predominately southwesterly winds, which is explained by Bodini [12] as impacted by the Martha's Vineyard land mass to the north and northwest of the lidar tower. The WHOI turbulence intensities are universally higher, especially from the north and northwest where the wind is blowing from the land with higher surface roughness generating more turbulence [12]. From the WP data, the turbulence intensity surpasses 0.08 only 15% of the time.

Figure 3-2 illustrates the impacts each wind condition has on the farm efficiency independently. Particularly at low wind speeds, farm efficiency significantly improves

with increasing TI (Figure 3-2a); it is probable that the wind speeds within the farm drop below the cut-in speed, precipitously lowering farm efficiency. A singular prescribed TI in a numerical model may not present the full importance of TI. Above the rated wind speed 10.6 m/s, however, wind speed dominates both TI and wind direction. Varying wind directions at speeds lower than the rated wind speed are vital to farm efficiency such that wake interactions are minimal. It should be noted that an unidentifiable bug our implementation of the FLORIS code made possible farm efficiencies greater than 100%; the efficiencies did not exceed 105% and should not detract from the relative impacts of each wind condition combination. This bug presented in even the simple case of a two-turbine array. While a solution was not reached before the publication of this thesis, we anticipate that this bug did not affect the qualitative results.

From Table 3.2, a major takeaway is that the means and medians for TI are similar if not identical. However, the histogram in Figure 3-3 illustrates significant differences in the probability distributions of TI between the datasets. While the WHOI TI peaks around 0.02 and gradually decreases in probability, the WP TI peaks at both 0.02 and 0.05. This distribution difference maps directly to the 4.40% difference in AEP between the two datasets, with WP AEP greater than WHOI AEP. The difference between the data is therefore larger than the medians would suggest. The 4.40% difference in AEP between the datasets at 140m, 225.53 GWh, is a significant over prediction by the WP data that negatively impacts a developer's LCOE since cost per unit energy will seem to be lower.

The purpose of the Monte Carlo analysis was to understand the possibility of using a fraction of the total datasets to predict AEP since the current FLORIS methods do not account for distributions of TI, and the additional code implemented is computationally expensive. Based on our findings, 5,000 random samples, approximately 15% of the datapoints, may be an efficient and accurate volume at which to run the wake model power calculations.

From a year's worth of data at 10-minute increments, 63% was viable from the WHOI dataset at 140m. It is possible comparing the full WP data to the existing

WHOI data (100% vs 63%) would result in larger or smaller differences, but that analysis was not done in this study.

4.2 Impact of Wind Conditions on AEP at Increased Hub Heights

Upon investigating the WP and WHOI datasets at different heights, the wind conditions did not change in the way that second research question of this thesis proposed. As seen in Tables 3.2, A.1, A.2, and A.3, the median turbulence intensities did not change with height for each dataset as well as between them. However, wind speed increased with height similar to the power law Equation 1.2. Since turbulence intensity is a relationship between TKE and wind speed (Equation 1.4), TKE must have increased proportionally to wind speed to maintain constant TI. Though TKE often decreases with height in onshore stable conditions, previous literature has not found a clear relationship between TKE and stability in the offshore environment [25].

Since turbine power increases with increasing wind speeds, it is not surprising that the AEP seen in Figure 3-8 increases with height. It is interesting to note the percent difference between the calculated AEPs decreases with height, which may be most directly impacted by the dominance of wind speed over other wind conditions above the rated wind speed. This also may be due to the WRF NWP more accurately predicting wind speeds higher in the ABL, versus the lower atmosphere that has a more complicated relationship with waves at the ocean surface [26].

4.3 Importance of Full TI Distribution vs Median TI

The results from the farm efficiency experiments shown in Tables 3.3 and 3.4 provide insight into the importance of the wind condition distributions when calculating farm efficiency and, similarly, AEP. Results from experiment 1), with median values for all three wind conditions, show the limitations of using a singular wind direction. Though median wind speed increased with height and median TI stayed constant for

each dataset, wind direction through the wind farm array determined the extent of the farm power. Figure 3-2 details the relationship of wind direction to farm efficiency, for which wind directions resulting in the most wake interaction had the lowest farm efficiency. For experiment 1), the WP farm efficiency is non-monotonic with height, and the WHOI farm efficiencies for 180m and 200m are significantly lower due to the median wind direction.

Although we performed the comparison between the WP and WHOI datasets with the full distributions of each wind condition, the results of farm efficiency experiments 2) and 3) show a small difference between using the full TI distribution versus using just the median TI. For all corresponding cases, the farm efficiencies were within 1.11% of each other. As noted in Tables 3.2, A.1, A.2, and A.3, the median TI was the same across all datasets at 0.04. The histograms (Figures 3-3, B-3, B-4, and B-5) comparing the distributions for TI between the datasets show a double peak for the WP data, and a smoother distribution for the WHOI data. Even with the interesting shape of the WP TI distribution, the median TI was still an efficient and accurate means of understanding the farm efficiency and AEP of the wind farm. Because this analysis was performed at a specific site for a single year, this comparison between median TI and the full TI distribution in farm power calculations may not hold everywhere.

Chapter 5

Conclusions

The goal of this thesis was to understand the impact that turbulence intensity has on AEP at the Vineyard Wind 1 farm and determine the importance of wind condition data sources on AEP. Based on the calculations of farm efficiency at different turbulence intensities, it can be concluded that TI has a direct impact on power and energy production. However, the calculated AEP using the full TI probability distribution at the Vineyard Wind 1 farm was less than a third of a percent different than the AEP calculated with the median TI.

Because it is expensive to directly measure wind conditions offshore at scale, it was important to compare the WHOI lidar measurements to the WP numerical weather prediction data. The WP AEP calculation was larger than that of the WHOI AEP at each hub height, though the percent difference decreased with height. Though the WHOI ASIT measurements are publically available for industry use, the data were not directly in the Vineyard Wind 1 lease area and were significantly impacted by the proximity to land. Although 4.40% AEP overprediction by WP compared to WHOI is significant, it is not certain that the WP wind condition predictions are not more accurate to the true values in the lease area, since the *in situ* measurements were not exactly at the WP coordinates. To understand the full AEP at the Vineyard Wind 1 site using the WP data, it is important to note that the WP data was filtered to directly match with the limited WHOI data; the WP data are available at every 5-minute interval from 2000 through 2020 and will continue to be updated. Year-to-year

uncertainties in wind conditions will also impact AEP values, though averages and trends may be understood with the extensive WP datasets available through NREL.

Though it was hypothesized that the turbulence intensity would decrease with height, this was not found to be the case for either dataset. Instead, TKE increased proportionally to wind speed, keeping TI constant. Therefore, the study could not assess the impact of changing turbulence intensity with height on AEP. As predicted, however, wind speed did increase with height and positively influenced the predicted AEP. The differences between the WP and WHOI AEP calculations decreased with height.

Because the United States has plans to broadly develop utility-scale wind farms across the Eastern Seaboard, it is the aim of this study to report the following: 1) turbulence intensity should be included in models as an important wind condition when designing the layout of a wind farm and considering wake interactions; 2) the NREL Wind Prospector Mid Atlantic Dataset is a valuable, inexpensive resource for data on the wind conditions in a given region without access to more accurate *in situ* measurements; 3) though using the median TI to calculate the AEP at the Vineyard Wind 1 site resulted in a difference of less than 0.33% compared to the AEP using the full TI distribution, the full TI probability distribution may be required for other sites and years of data to fully understand the wind energy potential there.

Bibliography

[1] Dvorak, Michael J., Cristina L. Archer, and Mark Z. Jacobson. California offshore wind energy potential.

[2] The White House. FACT SHEET: Biden Administration Jumpstarts Offshore Wind Energy Projects to Create Jobs, 29-03-2021.

[3] Barthelmie, R.J.; Dantuono, K.E.; Renner, E.J.; Letson, F.L.; Pryor, S.C. Extreme Wind and Waves in U.S. East Coast Offshore Wind Energy Lease Areas. *Energies*, 14, 2021.

[4] Roland B. Stull. *An Introduction to Boundary Layer Meteorology*. Kluwer Academic Publishers, 1988.

[5] Howland, Michael F., Sanjiva K. Lele, and John O. Dabiri. Wind farm power optimization through wake steering. *Proceedings of the National Academy of Sciences*, 116, 2019.

[6] Vineyard Wind 1. Nation's first commercial-scale offshore wind project.

[7] Paul Veers et al. Grand challenges in the science of wind energy. *Science*, 366, 2019.

[8] M. Akbar and F. Porté-Agel. Influence of atmospheric stability on wind-turbine wakes: A large-eddy simulation study. *Physics of Fluids*, 27, 2015.

[9] Amin Niayifar and Fernando Porté-Agel. Analytical Modeling of Wind Farms: A New Approach for Power Prediction. *Energies*, 9, 2016.

[10] Howland, Michael F., Aditya S. Ghate, Sanjiva K. Lele, and John O. Dabiri. Optimal closed-loop wake steering–Part 1: Conventionally neutral atmospheric boundary layer conditions. *Wind Energy Science*, 2020.

[11] K. Mansouri N. Charhouni, M. Sallaou. Realistic wind farm design layout optimization with different wind turbines types. *International Journal of Energy and Environmental Engineering*, 10, 2019.

[12] Nicola Bodini et al. U.S. East Coast Lidar Measurements Show Offshore Wind Turbines Will Encounter Very Low Atmospheric Turbulence. *Geophysical Research Letters*, 46, 2019.

[13] NREL. Floris. version 3.0.1, 2022.

[14] Paul Fleming et al. Field test of wake steering at an offshore wind farm. *European Academy of Wind Energy*, 2017.

[15] M.T. van Beek et al. Sensitivity and Uncertainty of the FLORIS Model Applied on the Lillgrund Wind Farm. *Energies*, 2021.

[16] S.B. Pope. *Turbulent flows*. Cambridge University Press, 2000.

[17] Alayna Farrel, Jennifer King, et al. Design and analysis of a wake model for spatially heterogeneous flow. *Wind Energy Science*, 6, 2021.

[18] Majid Bastankhah and Fernando Porté-Agel. Experimental and theoretical study of wind turbine wakes in yawed conditions. *Journal of Fluid Mechanics*, 806, 2016.

[19] A. Crespo and J. Hernandez. Turbulence characteristics in wind-turbine wakes. *Journal of wind engineering and industrial aerodynamics*, 61, 1996.

[20] Evan Gaertner et al. Definition of the IEA 15-Megawatt Offshore Reference Wind, 2020.

[21] Nicola Bodini. GRL offshore turbulence. GitHub, 2019.

[22] Dataset: Anthony R. Kirincich, Stephen M. Faluotico. Massachusetts Clean Energy Center MetOcean Data Initiative, 2019-04-04.

[23] C. Draxl, B.M. Hodge, A. Clifton, J. McCaa. The Wind Integration National Dataset (WIND) Toolkit. *Applied Energy*, 151, 2015.

[24] Jasmina L. Vujic. Monte Carlo Sampling Methods.

[25] Christakos, K., J. Reuder, and B. R. Furevik. Experimental characterization of the marine atmospheric boundary layer in the Havsul area, Norway. *Energy Procedia*, 35, 2013.

[26] Sara Porchetta, Domingo Muñoz-Esparza, Wim Munters, Jeroen van Beeck, Nicole van Lipzig. Impact of ocean waves on offshore wind farm power production. *Renewable Energy*, 180, 2021.

[27] Julian Quick et al. Wake steering optimization under uncertainty. *Wind Energy Science*, 5, 2020.

[28] Bureau of Ocean Energy Management. Vineyard Wind 1 Offshore Wind Energy Project Construction and Operations Plan.

[29] Cristina L. Archer and Ahmadreza Vasel-Be-Hagh. Wind farm hub height optimization. *Applied Energy*, 195, 2017.

[30] JF Herbert-Acero. A review of methodological approaches for the design and optimization of wind farms. *Energies*, 7, 2014.

[31] Majid Bastankhah and Fernando Porté-Agel. A new analytical model for wind-turbine wakes. *Renewable Energy*, 70, 2014.

[32] F. Blondel and M. Cathelain. An alternative form of the super-gaussian wind turbine wake model. *Wind Energy Science Discussions*, 2020.

[33] D. Dilip and F. Porté-Agel. Wind Turbine Wake Mitigation through Blade Pitch Offset. *Energies*, 10, 2017.

[34] Philipp Beiter Tyler Stehly and Patrick Duffy. 2019 cost of wind energy review, 2020.

Appendix A

Tables

	Wind Direction			**Wind Speed (m/s)**			**TI**		
	mean	median	σ	mean	median	σ	mean	median	σ
WP	211.8°	236.5°	98.1°	10.8	10.3	5.4	0.05	0.04	0.07
WHOI	210.5°	240.1°	101.9°	10.3	9.7	5.0	0.06	0.04	0.07

Table A.1: Statistics of the WP and WHOI wind condition data at 160m. Number of data point timestamps = 31037.

	Wind Direction			**Wind Speed (m/s)**			**TI**		
	mean	median	σ	mean	median	σ	mean	median	σ
WP	211.9°	238.2°	98.5°	11.0	10.5	5.4	0.05	0.04	0.07
WHOI	210.8°	242.5°	102.3°	10.6	10.1	5.2	0.06	0.04	0.07

Table A.2: Statistics of the WP and WHOI wind condition data at 180m. Number of data point timestamps = 27740.

	Wind Direction			**Wind Speed (m/s)**			**TI**		
	mean	median	σ	mean	median	σ	mean	median	σ
WP	209.0°	236.6°	98.1°	11.3	10.8	5.5	0.05	0.04	0.07
WHOI	209.2°	242.5°	101.7°	11.1	10.6	5.4	0.06	0.04	0.07

Table A.3: Statistics of the WP and WHOI wind condition data at 200m. Number of data point timestamps = 23555.

WP AEP (GWh)			
Hub Height	**1) Median TI, WS, WD**	**2) Median TI; Full WS & WD**	**3) Full TI, WS, WD**
140m	6982.36	5369.76	5355.21
160m	7258.32	5488.18	5471.95
180m	8000.31	5614.57	5599.25
200m	8189.42	5785.87	5771

Table A.4: AEP for the VW1 farm using the WP data at different hub heights. Farm efficiency 1) uses the median values for TI, wind speed (WS), and wind direction (WD); 2) uses the median TI with the full probability distributions of WS and WD; 3) uses the full probability distributions for TI, WS, and WD.

WHOI AEP (GWh)			
Hub Height	**1) Median TI, WS, WD**	**2) Median TI; Full WS & WD**	**3) Full TI, WS, WD**
140m	5555.26	5122.18	5129.68
160m	6215.44	5278.39	5292.25
180m	6003.48	5456.27	5473.93
200m	6948.00	5683.87	5702.06

Table A.5: AEP for the VW1 farm using the WHOI data at different hub heights. Farm efficiency 1) uses the median values for TI, wind speed (WS), and wind direction (WD); 2) uses the median TI with the full probability distributions of WS and WD; 3) uses the full probability distributions for TI, WS, and WD.

Appendix B

Figures

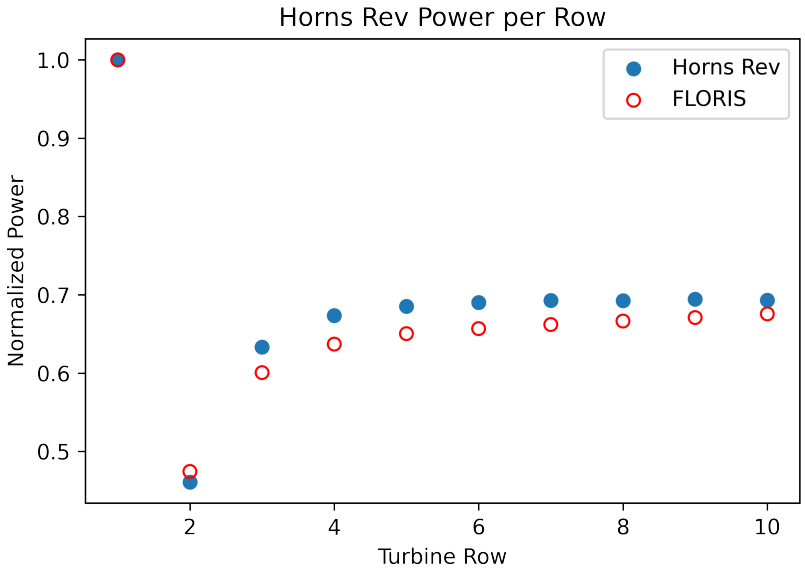

Figure B-1: Horns Rev normalized power per row from [9] compared to the calculated power from FLORIS.

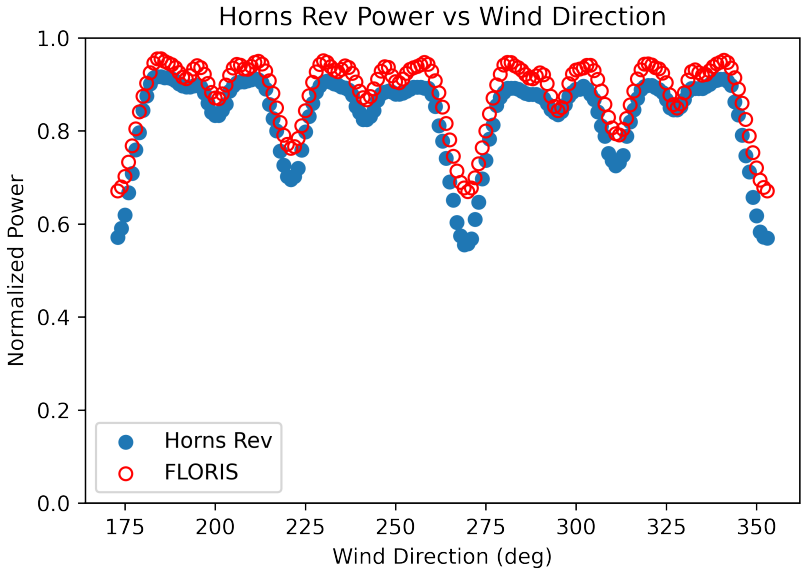

Figure B-2: Horns Rev normalized power versus wind direction from [9] compared to the calculated power from FLORIS.

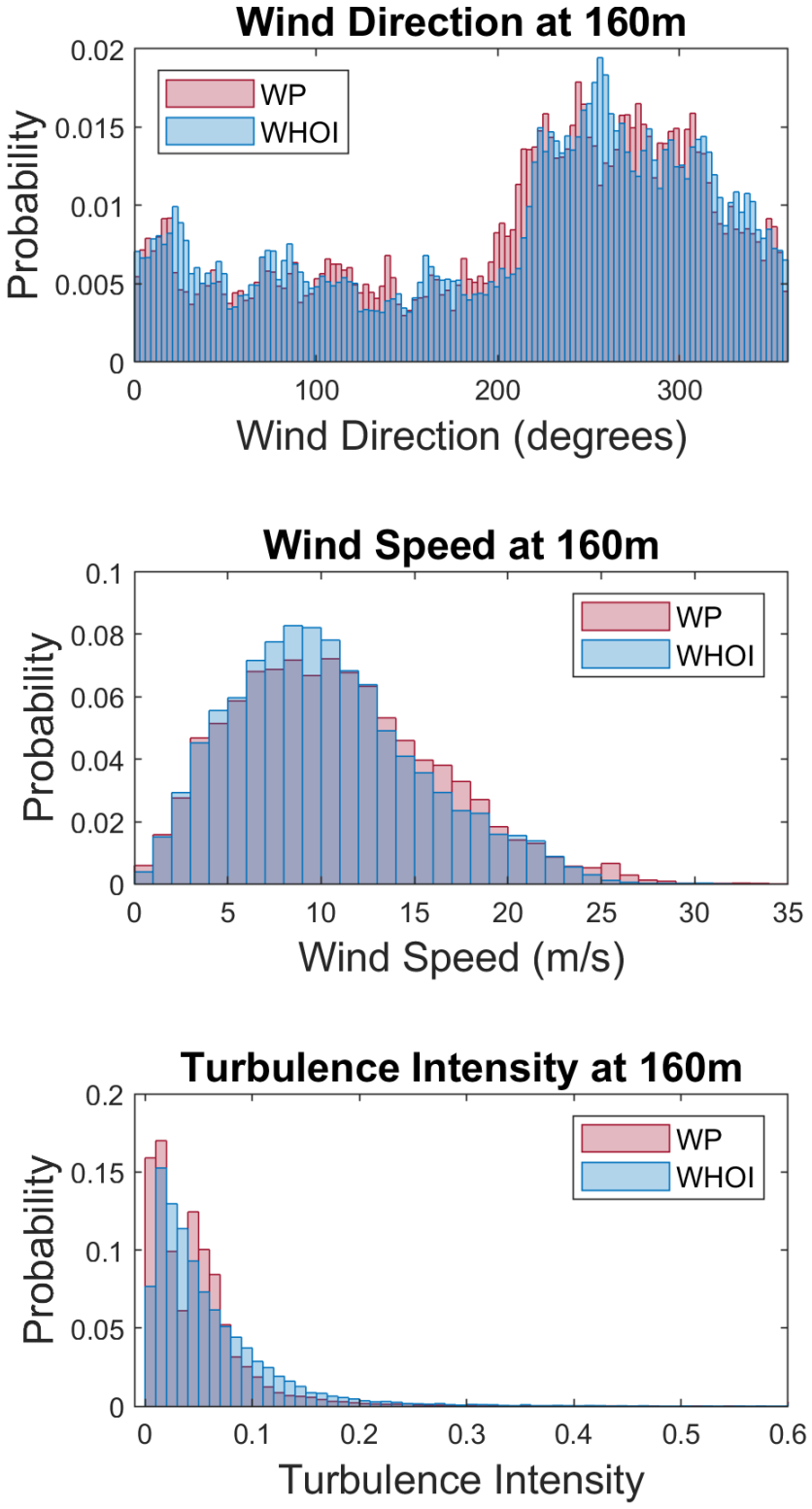

Figure B-3: Overlapping histograms of WP and WHOI data at 160m for wind direction, wind speed, and TI.

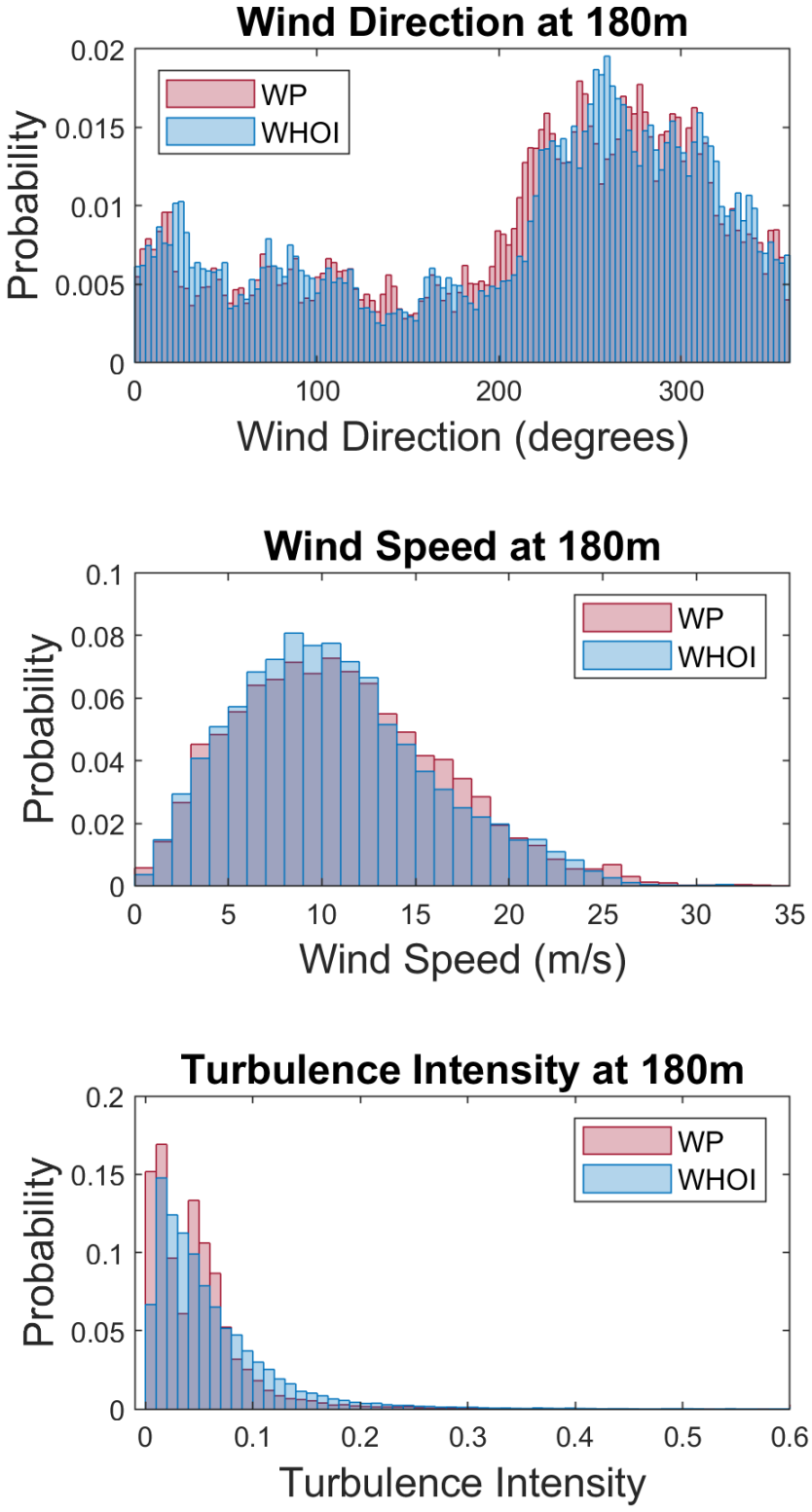

Figure B-4: Overlapping histograms of WP and WHOI data at 180m for wind direction, wind speed, and TI.

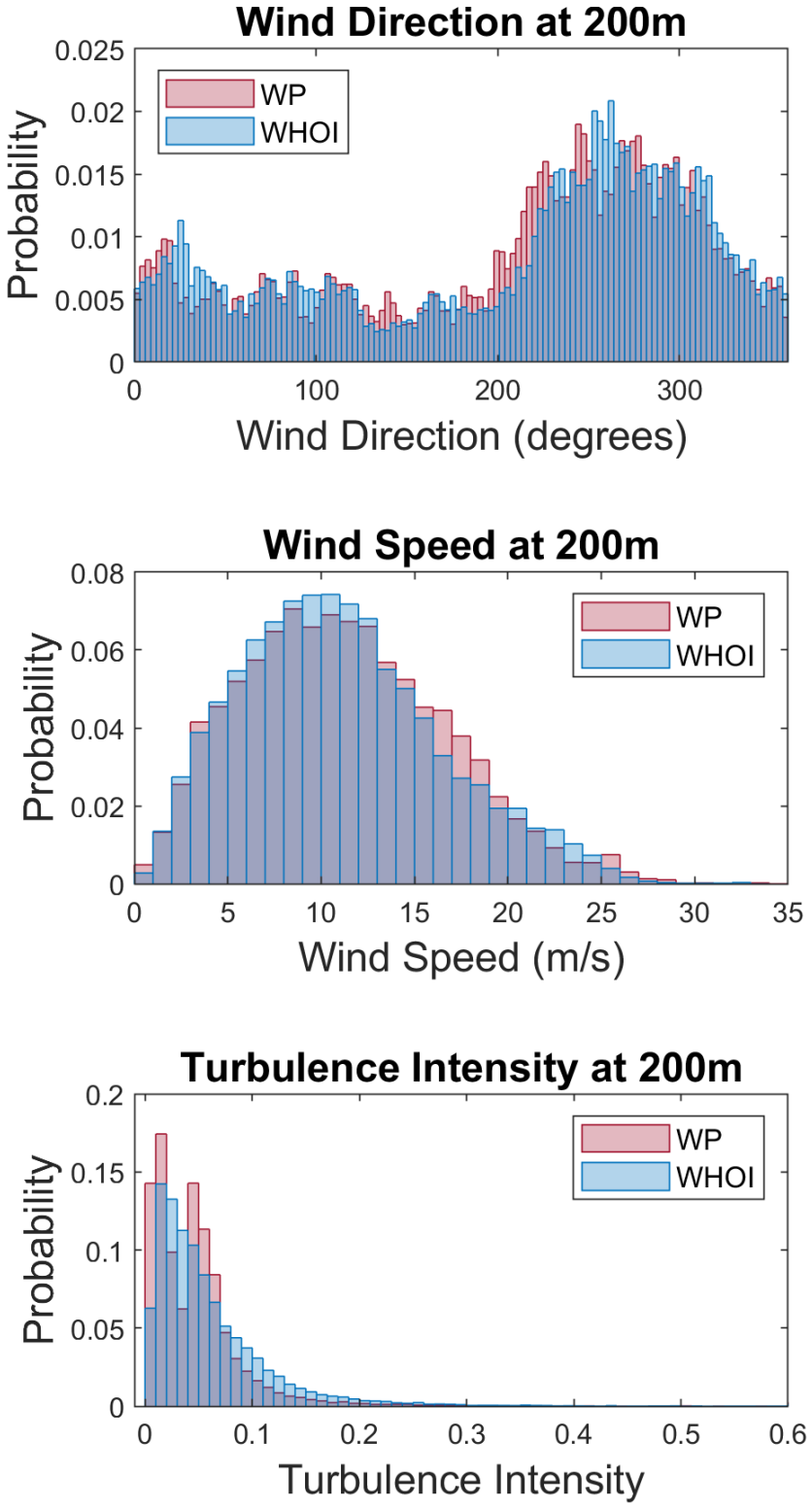

Figure B-5: Overlapping histograms of WP and WHOI data at 200m for wind direction, wind speed, and TI.